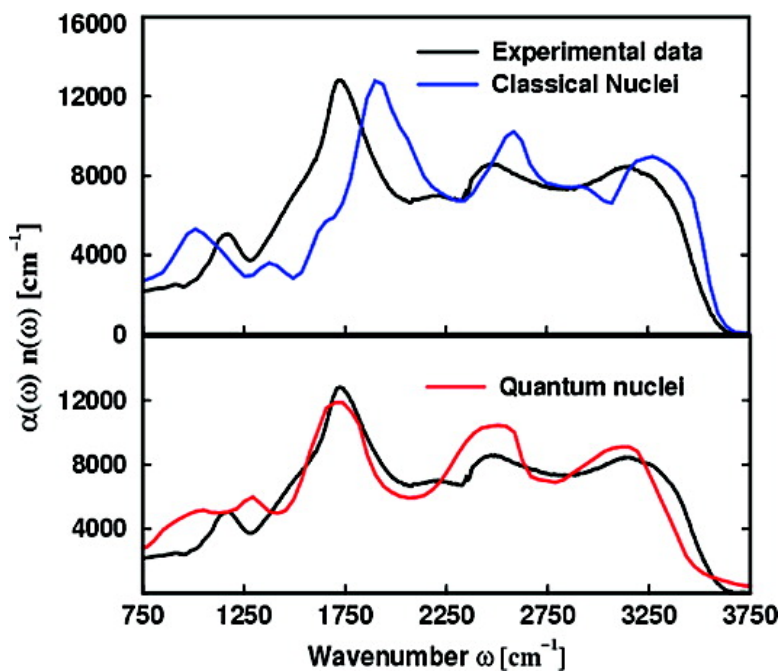


Spectral Signatures and Molecular Origin of Acid Dissociation Intermediates

Radu Iftimie, Vibin Thomas, Sylvain Plessis, Patrick Marchand, and Patrick Ayotte

J. Am. Chem. Soc., 2008, 130 (18), 5901-5907 • DOI: 10.1021/ja077846o • Publication Date (Web): 03 April 2008

Downloaded from <http://pubs.acs.org> on February 8, 2009



More About This Article

Additional resources and features associated with this article are available within the HTML version:

- Supporting Information
- Links to the 1 articles that cite this article, as of the time of this article download
- Access to high resolution figures
- Links to articles and content related to this article
- Copyright permission to reproduce figures and/or text from this article

[View the Full Text HTML](#)

Spectral Signatures and Molecular Origin of Acid Dissociation Intermediates

Radu Iftimie,^{*,†} Vibin Thomas,[†] Sylvain Plessis,[‡] Patrick Marchand,[‡] and Patrick Ayotte^{*,‡}

Département de Chimie, Université de Montréal, CP 6128, succursale Centre-Ville, Montréal H3C3J7, Canada, and Département de Chimie, Université de Sherbrooke, 2500 Boulevard Université, Sherbrooke J1K2R1, Canada

Received October 12, 2007; E-mail: radu.ion.iftimie@umontreal.ca; patrick.ayotte@usherbrooke.ca

Abstract: The existence of a broad, mid-infrared absorption ranging from 1000 to 3000 cm^{-1} is usually interpreted as a signature for the existence of protonated water networks. Herein, we use cryogenic mixtures of water and hydrogen fluoride (HF) and show experimental and computational evidence that similarly wide absorptions can be generated by a broad distribution of proton-shared and ion pair complexes. In the present case, we demonstrate that the broadening is mainly inhomogeneous, reflecting the fact that the topology of the first solvation shell determines the local degree of ionization and the shared-proton asymmetric stretching frequency within $\text{H}_2\text{O}\cdot\text{HF}$ complexes. The extreme sensitivity of the proton transfer potential energy hypersurface to local hydrogen bonding topologies modulates its vibrational frequency from 2800 down to $\sim 1300 \text{ cm}^{-1}$, the latter value being characteristic of solvation geometries that yield similar condensed-phase proton affinities for H_2O and fluoride. By linking the local degree of ionization to the solvation pattern, we are able to propose a mechanism of ionization for HF in aqueous solutions and to explain some of their unusual properties at large concentrations. However, an important conclusion of broad scientific interest is our prediction that spectral signatures that are normally attributed to protonated water networks could also reveal the presence of strong hydrogen bonds between un-ionized acids and water molecules, with important consequences to spectroscopic investigations of biologically relevant proton channels and pumps.

I. Introduction

Proton translocation constitutes a fundamental class of chemical transformations and is ubiquitous as an elementary process throughout nature. An important example is the conduction of protons along “water chains” in the transmembrane proton pumps of living cells.¹ Despite their fundamental role in chemistry and biology, insights into the microscopic mechanisms that facilitate proton transfer between Brønsted donors and acceptors are largely lacking. In particular, the nature of proton donor and acceptor intermediates relevant to various bioenergetics cycles is usually unknown, except for a few cases where significant progress^{2,3} has been recently reported.

Important insights into the dynamics⁴ and the thermodynamics⁵ of the proton translocation mechanism in hydrogen-bonded networks of various topologies can be gleaned from mid-infrared

(IR) spectra. Intermolecular proton transfer is thought⁶ to be facilitated to a large degree by solvent fluctuations and rearrangements, following a mechanism that is reminiscent of Marcus' picture⁷ of electron transfer reactions. The IR absorption spectrum is particularly revealing of these underlying microscopic details since it is extremely sensitive⁸ to the local H-bonding environment of the reactive groups involved. Specifically, shifts in the O–H stretching bands and in other localized vibrational marker modes along with observations of IR absorption continua are far more revealing of solvent dynamics for proton transfer reactions than the visible spectra.

However, the interpretation of IR spectroscopic investigations can be hampered by the difficulties in unambiguously assigning IR absorption patterns to specific local structures of a fluxional H-bonded network. These difficulties are particularly severe when investigating room-temperature aqueous solutions because of the large number of relevant solvation topologies^{9,10} and of their ultrafast dynamics.¹¹ Consequently, some of the most

[†] Université de Montréal.

[‡] Université de Sherbrooke.

(1) Decoursey, T. E. *Physiol. Rev.* **2003**, *83*, 475.

(2) (a) Garczarek, F.; Brown, L. S.; Lanyi, J. K.; Gerwert, K. *Proc. Natl. Acad. Sci. U.S.A.* **2005**, *102*, 3633. (b) Garczarek, F.; Gerwert, K. *Nature* **2006**, *439*, 109.

(3) (a) Mathias, G.; Marx, D. *Proc. Natl. Acad. Sci. U.S.A.* **2007**, *104*, 6980. (b) Rousseau, R.; Kleinschmidt, V.; Schmitt, U. W.; Marx, D. *Angew. Chem., Int. Ed.* **2004**, *43*, 4804.

(4) Mohammed, O. F.; Pines, D.; Dreyer, J.; Pines, E.; Nibbering, E. T. J. *Science* **2005**, *310*, 83.

(5) (a) Buch, V.; Milet, A.; Vácha, R.; Jungwirth, P.; Devlin, J. P. *Proc. Natl. Acad. Sci. U.S.A.* **2007**, *104*, 7342. (b) Buch, V.; Sadlej, J.; Aytemiz-Uras, N.; Devlin, J. P. *J. Phys. Chem. A* **2002**, *106*, 9374.

(6) (a) Ando, K.; Hynes, J. T. *J. Phys. Chem. B* **1997**, *101*, 10464. (b) Ando, K.; Hynes, J. T. *J. Phys. Chem. A* **1999**, *103*, 10398.

(7) Marcus, R. A. *J. Chem. Phys.* **1965**, *43*, 679.

(8) Zundel, G. *The Hydrogen Bond: Recent Developments in Theory and Applications*; Elsevier: New York, 1976.

(9) Marx, D.; Tuckerman, M. E.; Hutter, J.; Parrinello, M. *Nature* **1999**, *397*, 601.

(10) Schmitt, U. W.; Voth, G. A. *J. Chem. Phys.* **1999**, *111*, 9361.

(11) (a) Woutersen, S.; Bakker, H. J. *Phys. Rev. Lett.* **2006**, *96*, 138305. (b) Chandra, A.; Tuckerman, M. E.; Marx, D. *Phys. Rev. Lett.* **2007**, *99*, 145901.

successful recent efforts that attempted to clarify how the local H-bonding environment determines the IR spectral signature of the hydrated proton focused on gas-phase clusters^{12–14} and crystalline hydrates,¹⁵ employed ice surfaces at very low temperatures,^{5b} or relied on computational investigations.³

Amorphous aqueous solids at cryogenic temperature provide attractive alternative model systems for aqueous solutions as they can help trap metastable reaction intermediates in their liquid-like, albeit translationally static, disordered H-bonded networks. Moreover, while slowing down tremendously the collective solvent motions responsible for the ultrafast interconversion dynamics, investigations at very low temperatures may also allow valuable insight into subtle quantum nuclear effects which are obscured by thermal agitation in liquid solutions.

Herein, we investigate cryogenic mixtures of water and HF in order to explore the spectral signature of the transient structures that are involved in the process of ionization of HF molecules in aqueous solutions, leading to the formation of proton-shared intermediates and of contact ion pairs:



Dilute cryogenic solutions of HF in H₂O were recently shown¹⁶ to display the spectral signature of aqueous protons, similarly to the behavior observed for the strong acids HCl and HBr, suggesting a similarly extensive degree of ionization at 40 K in amorphous solid water. Entropic contributions could thus play an important role in determining the weak acid behavior of dilute hydrofluoric acid liquid solutions. Reflection–absorption infrared spectroscopy measurements are reported here for several concentrations, ranging from pure water to equimolar mixtures, in an attempt to provide a molecular level interpretation of the weak-to-strong acid behavior observed¹⁷ in HF aqueous solutions near equimolar concentrations.

First-principles molecular dynamics calculations of the Beer–Lambert absorptivity provide a detailed interpretation of the structure, dynamics, and vibrational spectra of various complexes found in equimolar cryogenic hydrofluoric acid solutions. Vibrational zero-point motions as well as incoherent tunneling effects are approximately included within the framework of the centroid molecular dynamics approach,¹⁸ resulting in an improved description of proton mobility and vibrational anharmonicity effects.

Our results indicate that the local degree of advancement of reaction 1 correlates well with the microscopic solvation environment, and also with the frequency of the shared-proton asymmetric stretching vibration. Hence, the extremely broad, experimentally observed absorption ranging from 1000 to 3400

cm⁻¹, the spectroscopic hallmark of polarizable¹⁹ hydrogen bonds in dilute solutions of strong acids, is attributed here to the large variety of microscopic solvation environments experienced by HF molecules in the amorphous binary solids. In particular, we demonstrate that the surprisingly broad and intense absorption extending from 1300 to 2000 cm⁻¹ that distinguishes the cryogenic¹⁶ from the room-temperature²⁰ mixtures signals the presence of proton-shared complexes F⁻·H⁺·OH₂ in which fluoride anions and water molecules display similar condensed-phase proton affinities. These proton-shared structures are intermediates in the ionization process depicted in reaction 1, being stabilized by distinctive first solvation shell H-bonding topologies and by long-range electrostatic interactions. In contrast, the spectral region ranging from 2000 to 2800 cm⁻¹ reveals the presence of the reactant and of the product species appearing in the ionization reaction 1, namely, weakly H-bonded HF molecules and contact ion pairs, respectively.

These observations suggest the existence of a supplementary level of complexity that needs to be considered in the interpretation of all disordered phase mid-IR experimental data. In particular, when weak Brønsted acids are present, care should be exercised when assigning specific mid-IR absorptions to the presence of protonated water networks. Our work demonstrates that spectroscopic features usually attributed to hydrated Eigen²¹ H₉O₄⁺ ions could also signal the presence of strongly hydrogen-bonded AH·OH₂ complexes between some weak Brønsted acid AH and a water molecule. In the same vein, we conclude that the appearance of broad and intense absorptions around 1800 cm⁻¹, similar to those that were recently identified in asymmetrically solvated gas-phase¹³ and transmembrane³ protonated water clusters, could also reveal the presence of undissociated O–H or N–H bonds that are stretched to the brink of ionization.

II. Results and Discussion

A. Cryogenic Mixtures of HF and H₂O Show Very Broad Absorptions That Differ from Those of Fully Dissociated Acids.

To set the stage, the lower panel in Figure 1 depicts the raw absorbance spectra measured at 80 K for 20 monolayers (ML) thick films of pure amorphous solid water (ASW; 0.0) for dilute (0.1) and for concentrated (0.5) homogeneous binary amorphous solid mixtures of HF, HCl, and HBr in H₂O having the same optical thickness as the ASW films. For the more diluted mixtures (0.1), a broad continuum of absorption is clearly observed across the 1000–3000 cm⁻¹ range in the raw spectra.

This is commonly recognized as the spectroscopic hallmark of aqueous protons. To better compare their absorption continua, difference spectra were computed for the dilute cryogenic aqueous mixtures using neat ASW spectra as reference (upper panel, top traces). Apart from differences in intensities, the absorption continua for the three dilute mixtures display striking similarities. Differences in the absorption continua are more pronounced in the more concentrated mixtures (0.5) where the cryogenic aqueous HF solutions display much larger intensities in the 1300–2500 cm⁻¹ range than the HCl and HBr mixtures (upper panel, bottom traces). The very similar spectra displayed by concentrated cryogenic hydrochloric (HCl) and hydrobromic (HBr) acid solutions suggest the presence of very similar molecular entities that differ substantially from those that can be found in concentrated cryogenic hydrofluoric acid solutions.

(12) Asmis, K. R.; Pivonka, N. L.; Santambrogio, G.; Brümmner, M.; Kaposta, C.; Neumark, D. M. *Science* **2003**, *299*, 1375.

(13) Headrick, J. M.; Diken, E. G.; Walters, R. S.; Hammer, N. I.; Christie, R. A.; Cui, J.; Myshakin, E. M.; Duncan, M. A.; Johnson, M. A.; Jordan, K. D. *Science* **2005**, *308*, 1765.

(14) Roscioli, J. R.; McCunn, L. R.; Johnson, M. A. *Science* **2007**, *316*, 249.

(15) (a) Delzeit, L.; Rowland, B.; Devlin, J. P. *J. Phys. Chem.* **1993**, *97*, 10312. (b) Buch, V.; Mohamed, F.; Parrinello, M.; Devlin, J. P. *J. Chem. Phys.* **2007**, *126*, 021102. (c) Buch, B.; Mohamed, F.; Parrinello, M.; Devlin, J. P. *J. Chem. Phys.* **2007**, *126*, 074503.

(16) Ayotte, P.; Hébert, M.; Marchand, P. *J. Chem. Phys.* **2005**, *123*, 184501.

(17) Hyman, H. H.; Kilpatrick, M.; Katz, J. J. *J. Am. Chem. Soc.* **1957**, *79*, 3668.

(18) Jang, S.; Voth, G. A. *J. Chem. Phys.* **1999**, *111*, 2371.

(19) Zundel, G. *Adv. Chem. Phys.* **2000**, *111*, 1.

(20) Giguère, P. A.; Turrell, S. *J. Am. Chem. Soc.* **1980**, *102*, 5473.

(21) Eigen, M. *Angew. Chem., Int. Ed. Engl.* **1964**, *3*, 1.

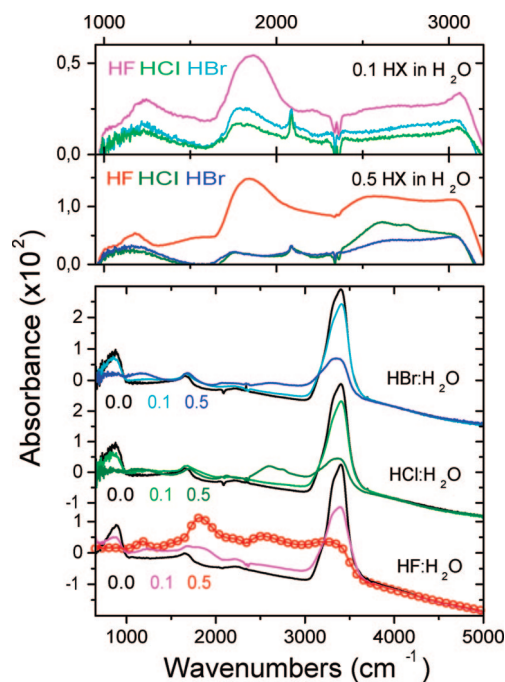


Figure 1. Lower panel: Raw reflection–absorption infrared spectra for 20 monolayers (ML) thick films of binary mixtures of hydrogen halides (HX; X = F, Cl, and Br) with H₂O at 80 K on Pt(111). Absorbance is reported as $-\log(I_{\text{film}}/I_{\text{p}})$ for 0.0 (neat amorphous solid water ASW), 0.1 (2 ML HX and 18 ML H₂O), and 0.5 (10 ML HX and 10 ML H₂O) homogeneous mixtures of HX with H₂O. The red line through the experimental spectrum (red circles) for 0.5 HF in H₂O displays model results using Fresnel relations to extract the optical constants reported in Figure 2. Upper panel: Difference spectra calculated using the ASW absorbance spectra from the lower panel as reference: $-\log(I_{\text{film}}/I_{\text{ASW}})$. While the absorption continuum displayed by dilute mixtures of HF in H₂O displays similarities to those of dilute HCl and HBr mixtures, spectra for concentrated HF aqueous solutions differ significantly from those observed for concentrated cryogenic mixture of the strong acids.

Much smaller differences between infrared spectra of room-temperature solutions of hydrohalic acids have previously been reported²⁰ by Giguère and his collaborators. These researchers concluded that the similarities between the broad conspicuous bands observed in the 1000–1400 and 1600–2000 cm^{-1} frequency ranges in the spectra of aqueous HF solutions with those observed in the strong acid HCl, HBr, or HI aqueous solutions should be interpreted as evidence for the existence of $\text{F}^- \cdot \text{H}_3\text{O}^+$ contact ion pairs. This model was proposed to provide a molecular-level interpretation for the weak acid behavior of dilute hydrofluoric acid solutions as resulting from the tying up of acidic protons in strongly bound ion pairs. The data displayed in Figure 1 show that lowering the temperature exacerbates the spectroscopic differences between hydrofluoric acid and the other hydrohalic acids.

Quantitative room-temperature investigations of the continuous absorbance generated by certain organic and inorganic acids led Zundel et al.²² and Chapados et al.²³ to suggest that undissociated acid molecules in water can capture a wide distribution of local H-bonded topologies similar to those characteristic of strong, fully dissociated acids. Progress in identifying the nature of the fluxional H-bond network in solutions of ionized, but undissociated, acids has been reported

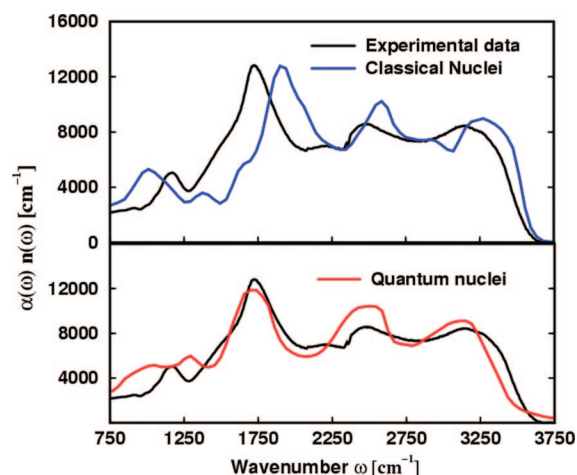


Figure 2. Absolute infrared absorption spectra of equimolar amorphous mixtures of HF and H₂O at 80 K. The experimental values (black trace) were obtained from raw reflection–absorption spectra by simulating the film–substrate system reflectivity using Fresnel relations and a value $n_{\infty} = 1.35$ for the optical index of refraction. Computational data were obtained using Car–Parrinello molecular dynamics in conjunction with either a Newtonian (blue trace) or an approximate quantum treatment (red trace) of the nuclear dynamics (see text). The excellent agreement between experiment and computation demonstrates that the chemical nature and concentration of the species that exist in our simulation box represent an adequate representation of the concentrated amorphous binary solid.

very recently by Iftimie and Tuckerman.²⁴ These authors found computational evidence suggesting that broad absorptions extending between 1000 and 1400 cm^{-1} could be attributed to Zundel-like proton-shared $\text{F}^- \cdot \text{H}^+ \cdot \text{OH}_2$ complexes. Furthermore, it was concluded that broad absorptions ranging from 2000 to 3000 cm^{-1} are consistent with the presence of stretched, but un-ionized, HF molecules that are strongly H-bonded to a water molecule forming a long-lived $\text{H}_2\text{O} \cdot \text{HF}$ complex.

However, the computational investigations by Iftimie et al.²⁴ suffer from a number of limitations that could potentially limit the validity and the generality of their conclusions. First, vibrational zero-point motion was not considered in that approach, which poses a fundamental problem in view of the fact that a vibrational mode at 1700 cm^{-1} that characterizes²⁵ certain relevant asymmetric double-well potentials with small activation barriers contributes a zero-point energy of $\approx 4 k_B T$ at ambient conditions. This supplementary energy could “lift” the proton above the underlying classical transition state and dramatically increase its delocalization. In the same vein, the errors introduced by the neglect of quantum corrections to classical anharmonicity effects were only approximately and inconsistently canceled by the use of finite basis set and fictitious electron mass, therefore limiting the reliability of the conclusions drawn from a direct comparison with the present experimental frequencies. Finally, the infrared signature of the $\text{F}^- \cdot \text{H}_3\text{O}^+$ contact ion pair limiting form was not revealed by that study of dilute solutions of HF in water, leaving open the possibility that this species might be the dominant one, as previously advocated by Giguère et al.²⁰

B. The Continuum of Absorption Is Generated by Heterogeneous Broadening of the Shared-Proton Asymmetric Stretching Frequency. In order to construct a detailed molecular-level model that can explain the experimental data displayed in Figure

(22) (a) Leuchs, M.; Zundel, G. *Can. J. Chem.* **1980**, *58*, 311. (b) Leuchs, M.; Zundel, G. *Can. J. Chem.* **1980**, *58*, 2118.
(23) (a) Max, J. J.; Chapados, C. *J. Phys. Chem. A* **2004**, *108*, 3324. (b) Max, J. J.; Chapados, C. *J. Phys. Chem. A* **2002**, *106*, 6452.

(24) Iftimie, R.; Tuckerman, M. E. *Angew. Chem., Int. Ed.* **2006**, *45*, 1144.
(25) (a) Roscioli, J. R.; Diken, E. G.; Johnson, M. A.; Horvath, S.; McCoy, A. B. *J. Phys. Chem. A* **2006**, *110*, 4943. (b) Yates, B. F.; Schaefer, H. F.; Lee, T. J.; Rice, J. E. *J. Am. Chem. Soc.* **1988**, *110*, 6327.

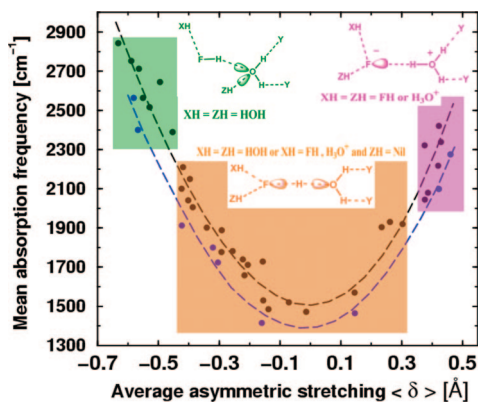


Figure 3. The mean infrared absorption frequency (filled circles) of shared-proton asymmetric stretching vibrations is correlated to the average value of δ (see text). The black points were obtained from classical simulations, while the blue ones correspond to centroid molecular dynamics data. The condensed-phase Brønsted basic character of the fluoride anion decreases during the ionization process. This decrease is correlated with changes in the number and the strength of the hydrogen-bond donors from the first solvation shell of the fluorine atom.

1, we performed classical Car–Parrinello²⁶ molecular dynamics simulations starting from five different initial atomic arrangements describing an equimolar amorphous mixture of HF and H₂O at 80 K. By comparing and contrasting computed and experimental infrared absorption spectra obtained at cryogenic temperatures, we were able to identify which system, among the five that were considered, most closely matched the experimental composition for the equimolar mixture. Subsequently, we focused on this system and recomputed its IR absorption spectrum by including nuclear quantum corrections within the context of the ab initio molecular dynamics implementation²⁷ of the centroid molecular dynamics¹⁸ theory.

With $\alpha(\omega)$ denoting the wavenumber-dependent Beer–Lambert absorptivity, $-1/l \cdot \ln(I/I_0)$, and $n(\omega)$ representing the index of refraction, Figure 2 compares the absolute values of the spectroscopic quantity $\alpha(\omega)n(\omega)$ that were computed from the raw reflection–absorption spectra of concentrated (0.5) amorphous mixtures of HF and H₂O at 80 K using our Fresnel reflectivity model to those obtained from first-principles molecular dynamics simulations. The excellent level of agreement between theory and experiment that is apparent from the results displayed in Figure 2 demonstrates that the microscopic composition of the system that was utilized in the first-principles simulations represents an adequate description of the amorphous binary solid prepared experimentally by simultaneous vapor condensation at 80 K using molecular beams. Moreover, the moderate magnitude of the nuclear quantum effects on the infrared spectra suggests that the data gathered in the present classical simulations can meaningfully be used to understand the molecular origin of the experimental infrared spectra. It is worth mentioning that this aspect was not obvious prior to the simulation since nuclear quantum effects as large²⁸ as 600 cm⁻¹ and anharmonicities on the order^{29,30} of 1000 cm⁻¹ had

previously been reported for the ionically H-bonded OH vibration in the chemically relevant gas-phase F⁻·H₂O system.

Using the five simulations equilibrated within the classical mechanics framework, we have computed the mean frequency and the width of the infrared absorptions generated by the very intense shared-proton asymmetric stretching vibration for all structures that could be described as reactants, intermediates, or products in reaction 1. We focused on these complexes as their very large transition dipole moments dominate the total infrared spectra. The vibration frequencies were computed using both the Newtonian and the approximate quantum (centroid) dynamics, and were tabulated as a function of $\delta = d(\text{F–H}) - d(\text{O–H})$, where $d(\text{A–B})$ is the distance between atoms A and B. The results obtained are shown in Figure 3 and suggest that the average value of the asymmetric proton stretch coordinate δ , which is a molecular measure of the degree of advancement of reaction 1, is strongly correlated to the shared-proton asymmetric stretching vibration frequency.

The correlation reported here is similar in spirit to the empirical relations found by Mikenda³¹ and by others³² between OH stretching frequencies and H-bond lengths in solids and should find numerous applications. In particular, the quantitative correlation reported in Figure 3 could allow experimentalists to “photograph” the ionization of HF in the same way in which Mikenda’s results helped in the interpretation of the pump–probe investigation³³ of the femtosecond dynamics of hydrogen bonds in liquid water. The broad distribution of δ values that was observed in the present simulations suggests that the chemical species appearing in reaction 1 are largely responsible for the continuous infrared absorption that ranges between 1300 and 2800 cm⁻¹. In the light of these data, the broadening appears to be largely inhomogeneous, being generated by a continuous distribution of metastable species sampling all intermediate geometries from the un-ionized FH·OH₂ to the contact ion pair F⁻·H₃O⁺ limiting structures.

C. A Mechanism for Acid Ionization and the Microscopic Solvent Reaction Coordinate for Proton Transfer by a Weak Acid. In order to complete the present picture of hydrogen fluoride ionization in water, one must include a description of the solvation effects that are responsible for shifting the equilibrium to the right in reaction 1. Visual investigation of the various proton transfer complexes obtained in our molecular dynamics simulations revealed an interesting correlation between the extent of proton transfer and the chemical nature of the first solvation shell, as illustrated in Figure 3. To understand the nature of this correlation, it is useful to divide the space of allowed values of the order parameter δ in three regions, corresponding to un-ionized, to proton-shared, and to contact ion pair complexes, as indicated in colors in Figure 3. One should bear in mind, however, that the precise definition of the boundaries separating proton-shared from un-ionized and from contact ion pair structures that was adopted in the present investigation is somewhat arbitrary. In particular, these boundaries are not dividing surfaces for slow, activated processes.

Using the ad hoc definition adopted in Figure 3, the first important observation that can be formulated is that un-ionized H₂O·HF complexes appear to be unevenly solvated, with the HF molecule in a single donor–single acceptor (DA) H-bonding

(26) Car, R.; Parrinello, M. *Phys. Rev. Lett.* **1985**, *55*, 2471.

(27) Marx, D.; Tuckerman, M. E.; Martyna, G. J. *Comput. Phys. Commun.* **2000**, *118*, 166.

(28) Schenter, G. K.; Garrett, B. C.; Voth, G. A. *J. Chem. Phys.* **2000**, *113*, 5171.

(29) Yates, B. F.; Schaeffer, H. F.; Lee, T. J.; Rice, J. E. *J. Am. Chem. Soc.* **1988**, *110*, 6327.

(30) Swalina, C.; Wang, Q.; Chakraborty, A.; Hammes-Schiffer, S. *J. Phys. Chem. A* **2007**, *111*, 2206.

(31) Mikenda, W. *J. Mol. Struct.* **1986**, *147*, 1.

(32) Novak, A. *Structure and Bonding*; Springer-Verlag: Berlin, 1974; p 177.

(33) Gale, G. M.; Gallot, G.; Hache, F.; Lascoux, N.; Bratos, S.; Leicknam, J. C. *Phys. Rev. Lett.* **1999**, *82*, 1068.

configuration, while the water molecule adopts a double donor–double acceptor (DDAA) binding motif. However, whenever a more symmetrical solvation pattern is reached, for example, by transferring a weak H-bond donating molecule from the accepting water oxygen to the fluorine atom yielding a AAD and a ADD configuration for HF and H₂O, respectively, a Zundel-like F⁻·H⁺·OH₂ shared-proton dissociation intermediate is formed. This result is consistent with the conclusions reached by Sillanpää et al.³⁴ who provided computational evidence suggesting that the fluorine atom increases its coordination number prior to the ionization of HF.

An interesting result that was revealed by the present low-temperature investigation is that proton-shared F⁻·H⁺·OH₂ complexes can occasionally be stable in a solvation environment in which the coordination number of the oxygen atom is larger than that of the fluorine atom. However, this can only happen if the fluorine is solvated by a powerful H-bond donating molecule, such as a hydrogen fluoride HF, or a hydronium ion H₃O⁺. In the same vein, it is important to mention that contact ion pairs of the form F⁻·H₃O⁺, in which the proton has transferred completely to the oxygen atom, were not stable in our simulations unless the fluoride anion was solvated by at least one and often two strong H-bond donating species. This observation is consistent with the ab initio molecular dynamics results previously reported by Iftimie et al.²⁴ and by Laasonen et al.³⁵ who were unable to find long-lived contact ion pairs F⁻·H₃O⁺ in dilute solutions. In order to understand these findings, let us start by noting that the extent of proton transfer is a direct measure of the local condensed-phase proton affinity difference between a fluoride anion and a water molecule.¹⁴ This proton affinity difference, which is largely in favor of the fluoride anion for the H₂O·HF cluster in the gas phase as its HF stretching frequency of 3633.8 cm⁻¹ testifies,³⁶ cannot change its sign unless the condensed-phase environment acts to significantly reduce the proton affinity of fluoride. Our results suggest that such a reduction is possible provided that at least one powerful H-bond donor (i.e., HF or H₃O⁺) and a weaker one (such as H₂O) are solvating the fluorine atom. Of course, it is highly improbable that such H-bonded topologies can be found in the first solvation shell of H₂O·HF complexes in binary solutions except in concentrated mixtures.

D. Assignment of the Experimental Spectral Features. We are now in a position to propose a detailed molecular-level assignment of the broad peaks that appear between 1300 and 3400 cm⁻¹ in Figure 2. Water molecules that are only solvated by weak H-bond donors and acceptors are exposed to an environment very similar to that of bulk water. Therefore, they are mostly responsible for the absorption that extends between 2800 and 3400 cm⁻¹. Un-ionized H₂O·HF complexes form stronger hydrogen bonds than those that are usually found in either pure water or pure HF and, according to the results displayed in Figure 3, absorb electromagnetic radiation between 2400 and 2800 cm⁻¹.

In contrast to the assignment proposed by Giguère²⁰ et al., our calculations suggest that F⁻·H₃O⁺ contact ion pairs in an amorphous environment absorb infrared radiation with wavenumbers that fall in the 2000–2400 cm⁻¹ range.

The results displayed in Figure 3 also indicate that H₂O·H⁺·F⁻ proton-shared species are largely responsible for the surprisingly intense absorption extending between 1300 and 2000 cm⁻¹. These Zundel-like shared-proton complexes are only stable in a disordered condensed phase and owe their existence to local environments in which fluoride anions and water molecules display comparable proton affinities. Inspection of the data in Figure 3 suggests that the structures that are responsible for these intense absorptions comprise FH or OH bonds on the verge of rupture, in which large amplitude proton motions and large vibrational transition dipoles are expected. It is therefore not surprising that these transitions display quantum anharmonic corrections amounting to a 200–300 cm⁻¹ red shift with respect to classical calculations, and that they are responsible for the largest features in the dipole autocorrelation spectra, while being hardly visible^{34,35,37} in velocity autocorrelation spectra.

Although the focus of the present work has been on the infrared spectra of the ion pairs appearing in reaction 1, no analysis of the spectroscopic properties of HF solutions is complete without mentioning the bifluoride FHF⁻ ions. Such ions are indeed present in our computational simulations of the amorphous equimolar mixtures, and an analysis of the infrared absorption generated by their shared-proton asymmetric stretching vibration reveals the presence of a broad absorption ranging from 1200 to 2000 cm⁻¹ whose maximum lies at 1600 cm⁻¹. These findings are consistent with the computational results³⁸ previously reported by Iftimie and Tuckerman for dilute solutions and with the experimental observations of KHF₂ solutions by Giguère et al.²⁰

III. Conclusions and Outlook

In an effort to understand the infrared signature of various ion pairs, we have conducted an investigation of amorphous binary mixtures of water and HF, HCl, or HBr at cryogenic temperatures. The absolute infrared spectra reported in the present investigation show the presence of extremely broad absorptions across the whole mid-IR range, which are usually considered to signal the presence of hydrated protons. We demonstrate that, in the case of cryogenic hydrofluoric acid solutions, a significant part of this broad absorption is generated not only by free protons but also by strongly hydrogen-bonded complexes between HF and H₂O, whose degree of ionization covers the entire spectrum from un-ionized species to contact ion pairs (see reaction 1). Moreover, our results suggest that the local extent of ionization can be understood in terms of how H-bonding topologies in the first solvation shell of H₂O·HF complexes affects the Brønsted acid–base properties of the fluoride anion and of the water molecule competing for the acidic proton.

As a general rule, the ionization process is promoted by a decrease in the condensed-phase proton affinity of the fluoride anion and by a concomitant increase in that of the water molecule. Our investigation reveals two mechanisms by which a fluoride ion can have its condensed-phase proton affinity decreased: either the number or the strength of the H-bond donating molecules from its first solvation shell must increase. In the same vein, we conclude that water molecules can increase their proton affinity either by decreasing their coordination

(34) Sillanpää, A. J.; Simon, C.; Klein, M. L.; Laasonen, K. *J. Phys. Chem. B* **2002**, *106*, 11315.

(35) Laasonen, K.; Klein, M. L. *Mol. Phys.* **1996**, *88*, 135.

(36) Bulychev, V. P.; Grigoriev, I. M.; Gromova, E. I.; Tokhadze, K. G. *Phys. Chem. Chem. Phys.* **2005**, *7*, 2266.

(37) Laasonen, K.; Larrucea, J.; Sillanpää, A. *J. Phys. Chem. B* **2006**, *110*, 12699.

(38) Iftimie, R.; Tuckerman, M. *J. Chem. Phys.* **2005**, *122*, 214508.

number from 4 (DDAA topology) to 3 (DDA topology) or by increasing the H-bond acceptor propensity of those molecules to which it is coordinated. A direct consequence of this proton transfer mechanism is that the overall degree of ionization is predicted to increase with increasing concentration of HF since these molecules can act as powerful H-bond donors. A larger degree of ionization will lead to an increase in the acidity constant as well as in the ionic mobility, therefore providing an alternative interpretation to the peculiar¹⁷ increase in acidity displayed by HF solutions of increasing concentration at room temperature.

Last, but not least, it is important to emphasize that the use of cryogenic temperatures has been instrumental to the successful completion of the present investigation. On one hand, the experimental spectra reported here show a significantly increased degree of ionization with respect to room-temperature data, allowing one to obtain reliable information about the behavior of ion pairs in dilute and concentrated solutions. On the other hand, the low thermal agitation ensures that atoms experience only moderate excursions about their quasi-equilibrium positions. Hence, the local degree of ionization and the composition of the first solvation shell do not change significantly on the computational simulation time scale, allowing one to investigate the relation between them, as well as their influence on infrared spectra.

IV. Experimental and Computational Methods

A. Experimental Approach. Nanoscopic ($h = 20$ ML ~ 7.5 nm) films of homogeneous HF:H₂O binary amorphous solids having various concentrations were prepared using simultaneous dosing with two molecular beams on a clean Pt(111) single crystal held at 80 K by a closed-cycle helium cryostat in ultrahigh vacuum. The molecular beam fluxes are calibrated using thermal desorption mass spectrometry of precisely controlled quantities of both species on Pt(111) from which we define one monolayer as the substrate saturation coverage (θ_{HF} and $\theta_{\text{H}_2\text{O}}$).¹⁶ Film compositions are reported in monolayer fractions = $\theta_{\text{HF}}/(\theta_{\text{HF}} + \theta_{\text{H}_2\text{O}})$. Their vibrational spectra were recorded at grazing incidence ($\theta_{\text{IR}} = 85^\circ$) using unpolarized light from a commercial FTIR spectrometer in a specular reflection-absorption geometry. Absorbance spectra for these ultrathin films present contributions from optical interference effects, as well as absorption, both of which are modulating the reflectivity of the substrate-film system. To minimize the optical distortions due to interference effects, we recorded spectra for films having the same optical thickness (i.e., $n_\infty \cdot h \cdot \cos \theta_{\text{IR}}$), but having different relative amounts of HF and H₂O. Absorbance spectra [i.e., $-\log R(\omega)/R_0(\omega)$] for our samples were numerically evaluated by calculating the reflectivity of the Pt(111) substrate [i.e., $R_0(\omega)$] and of the film-substrate systems [i.e., $R(\omega)$] using Fresnel relations. Empirical optical parameters [i.e., $k(\omega)$ and $n(\omega)$] were obtained iteratively by least-squares fitting simulated Fresnel spectra to experimental absorbance data. The incompleteness of the Kramers-Kronig transform has only negligible effects in the lower portion of the spectra (<700 cm⁻¹) due to poorer signal-to-noise. In our experiments, while the total number of layers deposited is very well-known and controlled very accurately, neither the absolute film thickness nor the density of the cryogenic solutions is known. Furthermore, the optical index of refraction is not known for aqueous solutions of HF at any temperature. A detailed sensitivity analysis of the Fresnel model was performed, and the best results were obtained by calculating the relative film thicknesses for different concentrations using the density of liquid hydrofluoric acid solutions and to determine the best optical index of refraction to match the cryogenic binary amorphous films' absorbance in the transparent portion of the spectra (i.e., 4000–8000 cm⁻¹).

A similar procedure was employed for mixtures of H₂O and HCl, or HBr. However, as these molecules dissociatively adsorb on Pt(111), we relied on the films optical thickness (i.e., interferometry) for molecular beam flux calibrations: 20 ML thick HCl or HBr films were defined as samples having the same interference pattern as that of a 20 ML thick amorphous solid water film in the transparent portion of the spectra (indices of refraction in the neat liquid phases are $n_\infty = 1.3287$ for HCl, 1.325 for HBr, and 1.33 for H₂O). The small and sharp features that appear near 2100 cm⁻¹ in the experimental spectra are due to trace CO chemisorbed on the Pt(111) substrate, and the doublet near 2350 cm⁻¹ is due to CO₂(g) in the purge gas.

B. Computational Methods and Their Accuracy. Herein we employ the Car-Parrinello²⁶ approach to describe electric polarization and bond-breaking/bond-forming effects. The simulations were performed using density functional theory,³⁹ the B-LYP generalized gradient exchange⁴⁰ correlation⁴¹ functional, plane wave basis sets, and norm-conserving Troullier-Martin⁴² pseudopotentials. The plane wave basis set cutoff was taken to be 100 Ry, and a fictitious electron mass $\mu = 246$ au in conjunction with an integration time step $\Delta = 0.06$ fs was utilized for the classical nuclei calculations. By taking room-temperature pure liquid water as a test case, we verified that the influence of the finite basis set and of the nonzero fictitious mass on the position of the maximum of absorption of room-temperature water was smaller than 40 cm⁻¹, which was the typical statistical resolution of the present classical simulations on the wavenumber axis.

Absolute infrared absorption spectra were computed from the trajectory of the total dipole moment using the Berry phase approach,⁴³ linear response theory,⁴⁴ and the Kramers-Kronig relations⁴⁴ using a practical method³⁸ recently developed by one of us. Zero-point vibration and hydrogen tunneling effects are included within the framework of the centroid¹⁸ molecular dynamics theory, which has been demonstrated⁴⁵ to significantly improve IR spectrum calculations beyond the so-called "harmonic approximation". Within the limits of applicability of the centroid molecular dynamics theory, Voth et al. have demonstrated¹⁸ that one can compute quantum time-autocorrelation functions by calculating single-time centroid symbol autocorrelation functions provided that the correlations involve operators that are linear combinations of Cartesian coordinates or momenta. Unfortunately, this is not the case for the electronic dipole moment, implying that a rigorous application of the centroid molecular dynamics theory should involve calculations of multiple-time⁴⁶ centroid symbol correlation functions, which are challenging to implement both at a theoretical and at a practical level in the present case.

The results displayed in Figures 2 and 3 were computed from the autocorrelation of an approximate dipole moment centroid symbol $\mathbf{M}_c(t)$, which was taken to be the instantaneous value of an average of classical dipole moments, with the average being taken over all path-integral quasi-particles:

$$\mathbf{M}_c(t) \approx \frac{1}{N} \sum_i \mathbf{M}(\mathbf{R}_i; t) \quad (2)$$

The magnitude of the approximation introduced by the use of eq 2 can be gauged from the results displayed in Figure 4, where the total infrared spectrum computed within the limits of the above-

(39) Koch, W.; Holthausen, M. C. *A Chemist's Guide to Density Functional Theory*; VCH: New York, 2000.

(40) Becke, A. *Phys. Rev. A* **1998**, *38*, 3098.

(41) Lee, C.; Yang, W.; Parr, R. G. *Phys. Rev. B* **1998**, *37*, 785.

(42) Troullier, N.; Martins, J. L. *Phys. Rev. B* **1991**, *43*, 1993.

(43) (a) King-Smith, R. D.; Vanderbilt, D. *Phys. Rev. B* **1993**, *47*, 1651.
(b) Vanderbilt, D.; King-Smith, R. D. *Phys. Rev. B* **1993**, *48*, 4442.

(44) Kubo, R.; Toda, M.; Hashitsume, N. *Statistical Physics II*, 2nd ed.; Springer: New York, 1991.

(45) Ramírez, R.; López-Ciudad, T.; Kumar, P.; Marx, D. *J. Chem. Phys.* **2004**, *121*, 3973.

(46) Reichman, D. R.; Roy, P. N.; Jang, S.; Voth, G. A. *J. Chem. Phys.* **2000**, *113*, 919.

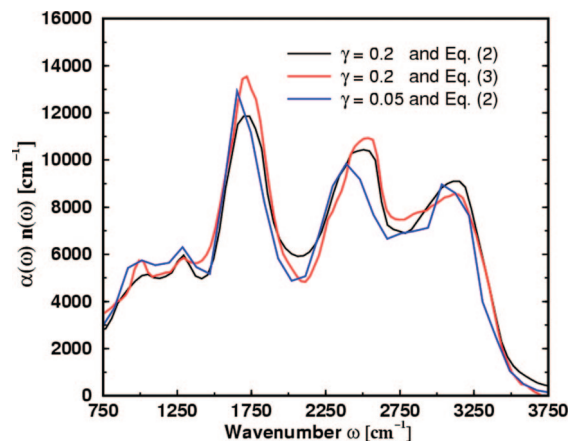


Figure 4. The total infrared spectrum of the amorphous monohydrate computed using the centroid molecular dynamics formalism (CMD) by assuming that the electronic dipole moment is a linear operator. Within this linear operator approximation, the dipole moment centroid symbol of the CMD formalism can be calculated by employing either eq 2 or 3 and the resulting autocorrelation spectra should be identical. The actual differences between the spectra computed by using eqs 2 and 3 are smaller than the statistical error bars of the simulation, suggesting that the electron dipole moment can approximately be treated as a linear operator without limiting the purpose of the present IR spectrum calculations. The figure also compares and contrasts the IR spectrum obtained with two values of the adiabaticity parameter γ (see text), suggesting that the magnitude of the nuclear quantum effects that can be deduced from Figures 2 and 3 are likely to be underestimated by 40–90 cm^{-1} .

mentioned approximation is contrasted with the IR results computed by approximating $\mathbf{M}_c(t)$ by the instantaneous value of the classical dipole moment

$$\mathbf{M}_c(t) \approx \mathbf{M}(\mathbf{R}_c; t) \quad (3)$$

where the vector \mathbf{R}_c stands for the center-of-mass (i.e., centroid) coordinates of the path-integral rings of quasi-particles:

$$\mathbf{R}_c = \frac{1}{N} \sum_i \mathbf{R}_i \quad (4)$$

These results suggest that the reliability of the quantum spectra displayed in Figures 2 and 3 is more likely to be limited by the fundamental approximation¹⁸ of the centroid molecular dynamics theory, as well as by its present practical implementation, and only to a smaller extent by the nonlinear nature of the electronic dipole moment operator.

The approximate quantum nuclei calculations were performed using 16 discrete path-integral¹⁸ replicas. The number of quasi-particles chosen in the present investigation represents a compromise between accuracy and computational cost, being consistently found close to the convergence limit in ab initio molecular dynamics investigations of similar systems: gas-phase $\text{F}^- \cdot \text{H}_2\text{O}$ clusters,^{28,29} gas-phase³⁰ and liquid-phase⁴⁷ HF multimers, and excess proton in liquid water.⁴⁸

A normal mode representation of path integrals was employed, with the centroid position of each atom defined as the zero-frequency mode of the corresponding quasi-particle chain. An adiabaticity parameter $\gamma = 0.2$ was employed following the suggestions of Marx²⁷ et al. based on their studies of gas-phase

quasi-harmonic (H_2) and relatively anharmonic (Li_2) diatomic potentials. Since this value of the adiabatic parameter is somewhat larger than the converged values (typically $\gamma = 0.06$) reported by Voth et al. in their studies^{48a,b} of excess proton in water, we have performed a shorter (2.0 ps), but significantly more computer-intensive, simulation with $\gamma = 0.05$ by starting from the same initial equilibrated configuration as the $\gamma = 0.2$ investigation.

The short duration of the simulation that employs the smaller value of γ limits the statistical resolution of the calculated infrared spectra to 90 cm^{-1} for the wavenumber axis and precludes a detailed analysis as the one shown in Figure 3. Nevertheless, one can see from the results displayed in Figure 4 that the total infrared spectrum computed by employing $\gamma = 0.05$ is quite similar to the one obtained with $\gamma = 0.2$, with estimated red shifts of 40 cm^{-1} for the broad absorptions centered at 1670 and 3200 cm^{-1} . The magnitude of this red shift is consistent with the one reported by Marx et al.²⁷ for similar changes in the value of γ and is insignificant within the statistical resolution of our $\gamma = 0.05$ simulation. In contrast, by reducing the value of the adiabaticity parameter γ , the absorption centered at 2450 cm^{-1} appears to be red shifted by 90 cm^{-1} . This value of the red shift is at the limit of resolution in our $\gamma = 0.05$ simulation and suggests that the quantum corrections to the proton stretching vibrational frequencies shown in Figures 2 and 3 might be slightly underestimated in the case of un-ionized $\text{H}_2\text{O} \cdot \text{HF}$ complexes.

We have ensured that the forces on the electronic coefficients remained as small in the centroid molecular dynamics calculations as they were in the Newtonian calculations by employing $\mu = 34$ au for the fictitious electron mass and $\Delta = 0.02$ fs for the integration time step in the $\gamma = 0.2$ simulation and by employing $\mu = 3.06$ au and $\Delta = 0.006$ fs in the $\gamma = 0.05$ simulation. All calculations were carried out using the PINY MD⁴⁹ simulation package. The simulations involved systems comprising 16 fluorine and 16 oxygen atoms and employed periodic boundary conditions. The dimensions of the simulation boxes respected the values of the respective system densities at room temperature. Classical simulations involved a relatively long annealing and equilibration period of 80 ps followed by data collection for 20 ps. Quantum simulations were equilibrated for 10 ps using the staging-variable implementation⁵⁰ of the imaginary time path integral ab initio molecular dynamics formalism, followed by data collection within the adiabatic centroid molecular dynamics approach. Data collection involved a period of 10 ps in the case of the $\gamma = 0.2$ and 2.0 ps in the case of $\gamma = 0.05$ simulation.

The data from Figure 3 were obtained by computing cross-correlation spectra between the trajectory of the total dipole moment and that of the normal mode $\delta = d(\text{F-H}) - d(\text{O-H})$ for selected pairs of fluorine and oxygen atoms, where $d(\text{A-B})$ represents the distance between atoms A and B (classical case) or that between their centroids (quantum case).

Acknowledgment. R.I. and P.A. acknowledge financial support from the Natural Sciences and Engineering Research Council of Canada, from the Fonds Québécois de la Recherche sur la Nature et les Technologies, and from the Canadian Foundation for Innovation. The Réseau Québécois de Calcul de Haute Performance is acknowledged for allowing us to perform the calculations.

JA0778460

(47) Raugei, S.; Klein, M. L. *J. Am. Chem. Soc.* **2003**, *125*, 8992.

(48) (a) Straus, J. B.; Calhoun, A.; Voth, G. A. *J. Chem. Phys.* **1995**, *102*, 529. (b) Wu, Y.; Chen, H.; Wang, F.; Paesani, F.; Voth, G. A. *J. Phys. Chem. B* **2008**, *112*, 467. (c) Tuckerman, M. E.; Marx, D.; Klein, M. L.; Parrinello, M. *Science* **1997**, *275*, 817.

(49) Tuckerman, M. E.; Yarne, D. A.; Samuelson, S. O.; Hughes, A. L.; Martyna, G. J. *Comput. Phys. Commun.* **2000**, *128*, 333.

(50) Tuckerman, M. E.; Marx, D.; Klein, M. L.; Parrinello, M. *J. Chem. Phys.* **1996**, *104*, 5579.